Hindawi
Advances in Civil Engineering
Volume 2018, Article ID 5920841, 11 pages
https://doi.org/10.1155/2018/5920841

Research Article

The Assessment and Evolution of Water-Conducting Rules under the Influence of Mining-Induced Stress

Feisheng Feng,[1,2] Suping Peng,[1] Wenfeng Du,[1,2] Yunlan He,[1,2] and Shan Chong[1,2]

[1]*State Key Laboratory of Coal Resources and Safe Mining, China University of Mining & Technology, Beijing, Beijing 100083, China*
[2]*College of Geoscience and Surveying Engineering, China University of Mining & Technology, Beijing, Beijing 100083, China*

Correspondence should be addressed to Suping Peng; psp@cumtb.edu.cn

Received 16 May 2018; Accepted 24 July 2018; Published 4 September 2018

Academic Editor: Hailing Kong

Copyright © 2018 Feisheng Feng et al. This is an open access article distributed under the Creative Commons Attribution License, which permits unrestricted use, distribution, and reproduction in any medium, provided the original work is properly cited.

It is important to study the mechanism of water inrush on a seam floor by exploring the rules of permeability variations during rock deformation on the seam floor and in the course of fracturing as well as their responses to characteristics of the macromechanical environment such as mine ground pressure, engineering geology, and fluid mechanics. First, through the analysis of bearing pressure changes in the process of exploiting the working face, a mechanical model for the seam floor above the confined water is established. Based on the graphic data-processing software Mathcad, the computational process and methods for assessing the vertical, horizontal, and shear stresses are provided together with the corresponding variation curve of the rock stratum 5 m below the floor, covering the entire process from a position 120 m away from the working face to a position 280 m behind it. Second, the permeability coefficients of different lithologies are measured in the laboratory. For rock stratum 5 m below the floor, the corresponding external loading path is set up according to its actual stress. The actual dynamic stress environment of the rocks is simulated, and their permeability characteristics are studied. In addition, based on data fitting, the permeability coefficient variations in the mining process are determined for a rock stratum 5 m below the floor. Finally, in accordance with the permeability variation law of the floor of the working face, the seam floor is divided into six areas, namely, the compression and expansion zone, the bed separation and expansion zone, the pressure relief zone, the compression zone, the stable recovery zone, and the stability zone. Thus, the water-resisting performance of the floor can be expressed more objectively.

1. Introduction

According to incomplete statistics, there were 181 water inrush accidents that occurred from 2001 to 2017 in China with 1,801 deaths and 73 people missing. During the four years from April 2013 to April 2017, there were 33 water inrush accidents that occurred on the floor, resulting in the deaths of 155 people. During the two time periods, the mortality rates were 42.8% and 45%, respectively, and indicated that the quantity of water inrushing on the floor has an impact on the degree of hazard of water inrush accidents. Massive studies on water inrush on the seam floor have been carried out by foreign and domestic scholars. In the 1940s, Слесарев [1] from the former Soviet Union believed that the seam floor was a clamped-clamped beam structure with a uniformly distributed load and derived a formula for designing a safe water pressure, as shown in the following equation:

$$P_0 = \frac{2K_p h^2}{L^2 + \gamma h}, \tag{1}$$

where P_0, h, and γ are the safe water pressure, thickness, and bulk density of the water-resisting layer of the floor, respectively; K_p is the tensile strength in MPa; and L is the roadway width in m. According to B. Slisalif, water inrush on the floor will occur when the actual water pressure $P > P_0$. According to mechanical equilibrium, the actual water inrush issue on the seam floor has been converted into a theoretical model, which lays a foundation for subsequent

theoretical development regarding the mechanism of water inrush on the seam floor.

By the 1980s, Santos and Bieniawski [2] had introduced dimensionless parameters m and s, which are relevant to the lithologic parameter and rock mass rating (RMR) on the basis of H-B criterion modification, thus further improving the expression of the floor loading capacity. It has also been noted that the ratio between the horizontal stress and the vertical stress of the floor could have an influence on floor security. In countries with a developed mining industry such as the United States and European countries, although there are many theoretical studies on rock mechanics and elastic-plastic mechanics, few have covered water inrush on the floor despite the simple seam structure and advanced mining facilities. From the 1960s to the 1970s, the water inrush coefficient T (shown in Equation (2)) as well as its modified formula T_c (shown in Equation (3)) was brought forward by Chinese scholars and institutions [3, 4]:

$$T = \frac{P}{H}, \tag{2}$$

$$T_c = \frac{P}{\sum\left(h_i a_i - h_p\right)}, \tag{3}$$

where H is the total thickness of the water-resisting layer of the floor; h_i is the stratification thickness of the ith water-resisting layer; h_p is the depth of the floor destroyed by ground pressure; and a_i is a thickness coefficient representing the transition of the ith water-resisting layer to mudstone, the value of which ranges from 0 to 1. The water inrush coefficient is gradually becoming an important reference for water-proofing work in coal mines in China.

In 1980, Baiying [5–7] explored coal mining below confined water with Ordovician limestone, proposing the "Three Underlying Belts Theory," a schematic diagram of which is shown in Figure 1. The formula for computing the water inrush coefficient based on this theory is shown in Equation (4).

Because of the division of three underlying belts, the formula for computing the water bursting coefficient can be modified into the equation as follows:

$$T = \frac{P}{\left(H - H_1 - H_3\right)} = \frac{p}{H_2}, \tag{4}$$

where T stands for the water inrush coefficient. H, H_1, H_2, and H_3 represent the total thickness and the thicknesses of belts 1, 2, and 3, respectively. The Three Underlying Belts Theory emphasizes that the floor has a structure similar to the three belts of an overburdened roof. It also notes that the floor failure mechanism can be described as the process of water inrush on the aquifer floor caused by the communication between the mining fissure zone and the aquifer under the combined action of water pressure and mine ground pressure.

At the beginning of the 20th century, a modified formula for water pressure reduction was proposed by Hu and Yan [8] and Weiyue et al. [9, 10] based on the Three Underlying Belts Theory. Specifically, head pressure subjected to an

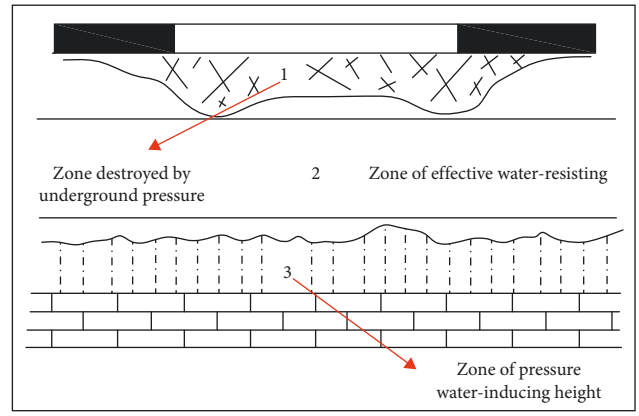

Figure 1: Schematic diagram of the Three Underlying Belts Theory.

effective water-resisting seam floor will show pressure loss due to water head intrusion. A schematic diagram of the pressure loss in the aquifer is given in Figure 2. The formula for computing the water inrush coefficient based on water pressure loss in the aquifer is shown in Equation (6).

P_c represents the water pressure after the reduction. More factors influencing the hydraulic mining of the coal seam have been taken into account after the improvement, including not only the zonation of the water-resisting layer on the seam floor but also the residual water pressure, which is likely to be neglected. As a result, the modified formula for the water inrush coefficient can help us to more faithfully and effectively evaluate the security of hydraulic mining, benefitting the practice of mining. Additionally, according to the in situ fissure and original destruction theory raised by Zuoyu et al. [11–13], the horizontal influence of the water-resisting layer on the actual working face of the mine is mainly divided into the advanced pressure compression section, the pressure relief-based expansion section, and the postmining stable compression section because of the joint effect of the mine pressure and the hydraulic pressure. According to the key stratum theory raised by Minggao et al. [14, 15], there is a key stratum similar to the overlying stratum on the roof on the seam floor, and this stratum is the main inducer of water inrush on the seam floor during hydraulic mining in the control belt. Using an analytic hierarchy process (AHP) and geographic information system (GIS), Wu et al. [16, 17] proposed the brittleness index method and established an AHP evaluation model to define the threshold of each risk level to guide the operation of mining areas. Peng et al. [18] have combined double-unit face mining technology and strip mining and performed studies on coal mining above the confined water, guaranteeing the safety of mining upon confined water from the perspective of mining technology. The in situ measurement conducted by Huang et al. [19] targeted the permeability of the fractured zone on the floor in Yangcun Coal Mine and Xinglong Zhuang Coal Mine in Shandong Province of Eastern China. The rock permeability and the permeability variation under conditions of varied water pressure were measured; Meng et al. [20] established a coal floor water inrush risk assessment method based on a conventional

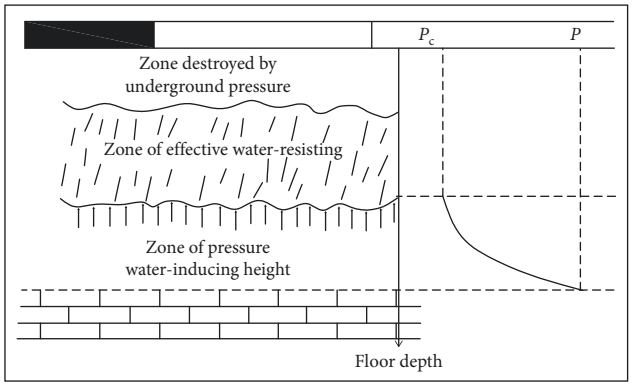

Figure 2: Schematic diagram of water pressure loss in the aquifer.

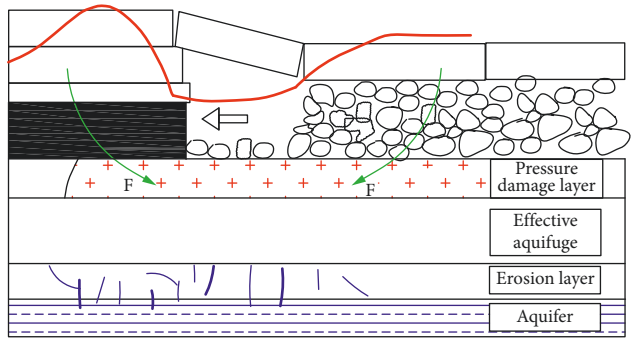

Figure 3: Floor structure and stress distribution in goaf.

water inrush coefficient, considering the lithology and structure features; Wang et al. [21] established a novel comprehensive evaluation model based on the normal cloud theory for solving the randomness and fuzziness in the evaluation process of water inrush risk; Ma et al. [22] established a new rock test system to study the migration of small particles of granular sandstone samples under different original porosity, particle size composition, and water flow pressure; Kang et al. [23] constructed 3-D numerical simulation of groundwater flow to predict the water gushing during coal mining due to the impact on the aquifer caused by the crack zones; Wang et al. [24] studied the permeability change of mining fissured rock mass and its effect on groundwater inrush. Liu et al. [25, 26] studied the mechanical characteristics of the rocks from multiple scales, and particularly they made analysis and prediction of rock hydraulic properties under water-rock coupling from a microperspective, providing new ideas and methods for researches on water inrush from seam floor.

Practical studies suggest that floor seepage is an extremely complex water-rock coupling issue triggered by characteristics of the macromechanical environment such as mine ground pressure, engineering geology, and fluid mechanics. In this paper, a mechanical model of floor stress has been established to describe dynamic variations in the floor stress during the dynamic stress variation of the working face. Permeability characteristics have also been measured in the laboratory under conditions of diverse stress states. Specific to rules of rock permeability change in the entire stress-strain process on the working face, the seam floor is divided into six zones, that is, the compression and expansion zone, the bed separation and expansion zone, the pressure relief zone, the compression zone, the stable recovery zone, and the stability zone. In this way, the water-resisting performance of the floor is represented more objectively.

2. Materials and Methods

2.1. Analysis of the Stress State Distribution on the Floor of the Slope. In regard to mining upon confined water, the stress state distribution on the roof is given in Figure 3. The reason that curves in areas with low stress from primary rock are longer than those in traditional mining-induced stress zones is that a masonry structure is formed by overlying strata, creating a stress vacuum area with a length approximately equal to a periodic weighting step [27, 28]. The area exists between the goaf caving end and the elastic zone of the working face. For the convenience of calculation, the curve was simplified into a triangle. Then, stress variation could be expressed as $\Delta\sigma_y = \sigma_{\text{upper}} - \sigma_{\text{lower}}$. Selecting A as the coordinate center, the coordinate of any point denoted by M$(m, -n)$ was taken within the carmine box. Furthermore, the floor was assumed to be homogeneously elastic, and a numerical calculation model for the floor stress distribution was established, as presented in Figure 4.

As assumed, mining was not completed until periodic weighting; in which case, the stress of the mine supporting pressure in an area to the right of point M can be expressed in the following equation:

$$\begin{cases} d\sigma_x = -\dfrac{2pd\xi}{\pi}\dfrac{x^3}{\left[x^2+(y-\xi)^2\right]^2} \\ d\sigma_y = -\dfrac{2pd\xi}{\pi}\dfrac{x(y-\xi)^2}{\left[x^2+(y-\xi)^2\right]^2} \\ d\tau_{xy} = -\dfrac{2pd\xi}{\pi}\dfrac{x^2(y-\xi)}{\left[x^2+(y-\xi)^2\right]^2} \end{cases} \Longrightarrow \begin{cases} \sigma_x = -\dfrac{2}{\pi}\displaystyle\int_{y_1}^{y_2}\dfrac{p(\xi)x^3\,d\xi}{\left[x^2+(y-\xi)^2\right]^2} \\ \sigma_y = -\dfrac{2}{\pi}\displaystyle\int_{y_1}^{y_2}\dfrac{p(\xi)x(y-\xi)^2\,d\xi}{\left[x^2+(y-\xi)^2\right]^2} \\ \tau_{xy} = -\dfrac{2}{\pi}\displaystyle\int_{y_1}^{y_2}\dfrac{p(\xi)(y-\xi)x^2\,d\xi}{\left[x^2+(y-\xi)^2\right]^2}. \end{cases} \tag{5}$$

The normal stress presented in Figure 4 is divided into 4 sections, AB, BC, CD, and DE. Taking Haizi Coal Mine in Anhui Province as an example, both the geological conditions of the working face and the behavior of the mine ground pressure measured during working face advance are obtained, where the length of S1 and S2 is 10 m and 30 m, respectively; the stress concentration factor K is equal to 2.5; the length $L2$ is 10 m; and the distance from the working face to the origin of the coordinates is 40 m. By using Mathcad as the mathematical analysis software, section AB was solved first:

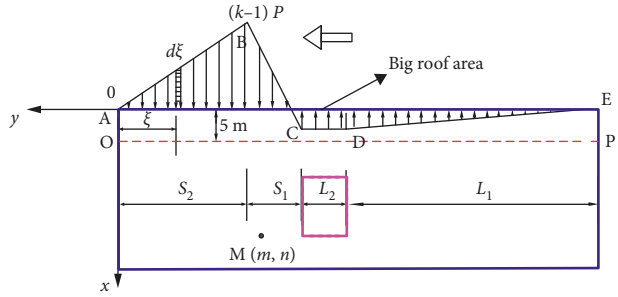

Figure 4: Bearing pressure distribution of the floor upon confined water.

$$\sigma_{x1}(y) = -\frac{2}{\pi}\int_{-30}^{0}\frac{(-0.05\xi)x^3}{\left[x^2+(y-\xi)^2\right]^2}d\xi = -0.0159\left[x + y\arctan(xy)\right] + 0.0159\left[\frac{30xy + x^3 + xy^2 + y\arctan(30+y)x + y^3V_1 + 60y^2V_1 + 900yV_1}{V_2}\right],$$

$$\sigma_{y1}(y) = 0.0159x\left[1+\ln\left(x^2+y^2\right)\right] - 0.0159y\arctan\frac{y}{x} - 0.0159\left[\frac{30xy + x^3 + xy^2 - y\arctan(30+y)x - y^3V_1 - 60y^2V_1}{V_2} + \frac{-900yV_1 + x^3\ln V_2y^2 + 60x\ln V_2y + 900x\ln V_2}{V_2}\right],$$

$$\tau_1(y) = 0.0159x\arctan\left(\frac{y}{x}\right) - 0.0159x\left[\frac{-30x + \arctan(30-y)x + y^2V_1 + 60yV_1 + 900V_1}{V_2}\right]. \quad (6)$$

Subsequently, solutions to sections BC, CD, and DE were acquired. In this context, the stress distribution law of the stress increment bearing pressure on the floor along the working face could be further obtained. V_1 and V_2 can be obtained as follows:

$$V_1 = \arctan\left(\frac{30+y}{x}\right),$$
$$V_2 = x^2 + y^2 + 60y + 900. \quad (7)$$

2.2. Laboratory Studies. Rock specimens were acquired from the working face floor. To prevent the influence of lead abutment pressure, rock specimens of different rock formations were selected on the roadway floor at the layout and open-off cut stage of the working face, including coal, mudstone, sandstone, and sandy shale. Relevant specimens are cylinder-shaped, and 5 should be processed specific to each category of rock. For the standard specimen size selected, $H = 100$ mm and $d = 50$ mm, where H refers to height and d refers to the diameter of the section.

An RTR high-temperature high-pressure rock triaxial apparatus manufactured by GCTS and adopted for the experiment could complete rock permeability coefficient measurements at different confining pressures. Based on computer process control, the preset confining pressure loading scheme was implemented in an unceasing manner targeted at the same specimen.

The main research elements are as follows:

(1) Rock permeability variation law in a complete stress-strain path

(2) Rock permeability variation law subjected to different confining pressures

(3) Rock permeability variation law subjected to a particular loading path

3. Results and Discussion

(1) The permeability variation rules in a complete stress-strain path were investigated since excessively low confining pressure may affect the related experimental effects. Meanwhile, the specimen depth, position, stress conditions, and so on were all taken into account. The corresponding confining pressure was set as $P_c = 4$ MPa.The laboratory apparatus and specimens utilized are presented in Figures 5. Figure 6 is the schematic diagram of the concrete measurement principle.

With regard to rocks of different types of lithology, their permeability coefficient (K) variation curves with stress ε are given in Figure 7.

Figure 5: Picture of the experimental apparatus.

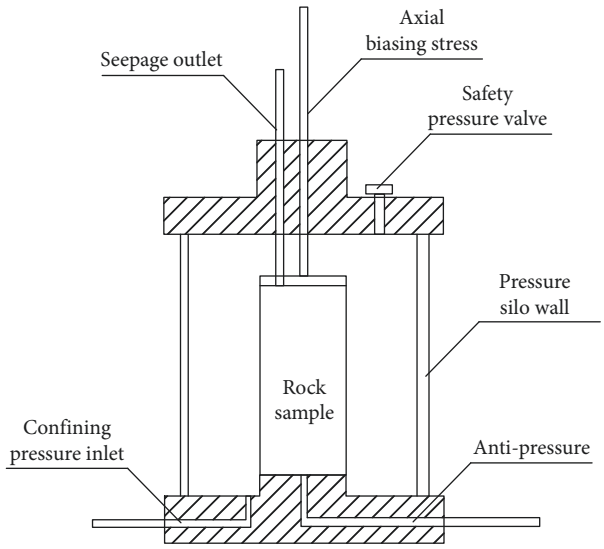

Figure 6: Schematic diagram of measurement principle.

The permeability of four kinds of rocks slightly decreases with the increase in stress at the very beginning (at the stage of initial crack closure) or has no obvious change (initial cracks not developed) [29, 30]. It increases slightly as the load increases before reaching the peak intensity. At the elastic-plastic stage, rocks go through dilated deformation and crack holing starts. The rock permeability coefficient arrives at its peak value at the postpeak phase and is reduced in the remaining stages. What is noteworthy is that the peak of the permeability coefficient falls behind that of rock strength. Therefore, strain softening supervision and control after rock failure have critical significance for preventing water bursting on the seam floor. In the condition of identical confining and seepage pressure, rocks can be ranked as coal, sandy shale, sandstone, and mudstone in the descending order according to their permeability. Respectively, they take values of 128, 52.38, 27.90, and 0.048 unit(s) defined as $\times 10^{-10}\,\mathrm{m{\cdot}s^{-1}}$.

At the very beginning, permeability slightly increases and decreases with the increase of stress for the mudstone, which is different from other rock samples. The reason is the relatively large fissures within the other rock samples narrow with the increase of axial pressure, leading to a slightly decreased permeability, while there is not a similar process for mudstone within which the fissures are small. The increase of axial pressure will create small fissures within mudstone, and more increment will lead to interior fracture; detritus thereby produced will block the permeation channels resulting in a temporary reduction of the permeability.

With further increase of axial pressure, the degree of fracture aggravates, and the permeability increases rapidly.

(2) Specific to rock permeability variation rules subjected to different confining pressures, the peak strain ε_{max} of the rock specimens was first achieved by loading. Then, in the conditions of diverse confining pressures, namely, $P_c = 1.5$ MPa, 2 MPa, 3 MPa, 4 MPa, 6 MPa, 8 MPa, 10 MPa, 12 MPa, and 14 MPa, the corresponding permeability coefficients denoted as K were determined. At the beginning of the experiment, the confining pressure increases from 1 MPa. When the experiment is complete, the rubber membrane around the rock specimen should be checked. A damaged rubber membrane indicates that the confining pressure adopted during the experiment was excessively low and the test should be valid since the confining pressure P_c is equal to 1.5 MPa.

Subjected to diverse confining pressures, the permeability variation rules of different rocks are presented in Figure 8.

As demonstrated by the experiment, the permeability coefficient is closely related to the confining pressure. The greater the confining pressure is, the lower the permeability will be. Meanwhile, all four kinds of rocks with relevant values of 0.9 and above show a rule of multinomial distribution. It has been found by Peng et al. [31] according to their investigations on rocks from diverse geologic ages that a logarithmic relation exists between them; in fact, their variation rules are consistent. Furthermore, the relation between permeability and confining pressures can be expressed in the equation below:

$$K = a + bP_c + cP_c^2, \tag{8}$$

where K refers to the permeability coefficient, P_c refers to the confining pressure, and parameters a, b, and c are all constants.

Comparatively speaking, coal permeability is the most sensitive to the influence of confining pressure, while the sensitivity of rock permeability at the postpeak phase to the influence of confining pressure ranks last. At the time of coal mining, the permeability coefficients of coal and rocks beneath it increase. However, the great water-resisting property of mudstone guarantees floor safety. Despite the fact that an increase in mudstone permeability is accompanied by a substantial increase in the probability of the seam floor water bursting, the water-resisting performance in the upper part of the mudstone plays a critical role in improving the confining pressure on the water-resisting layer at the bottom, which has been proven by the theoretical model in Part One. The

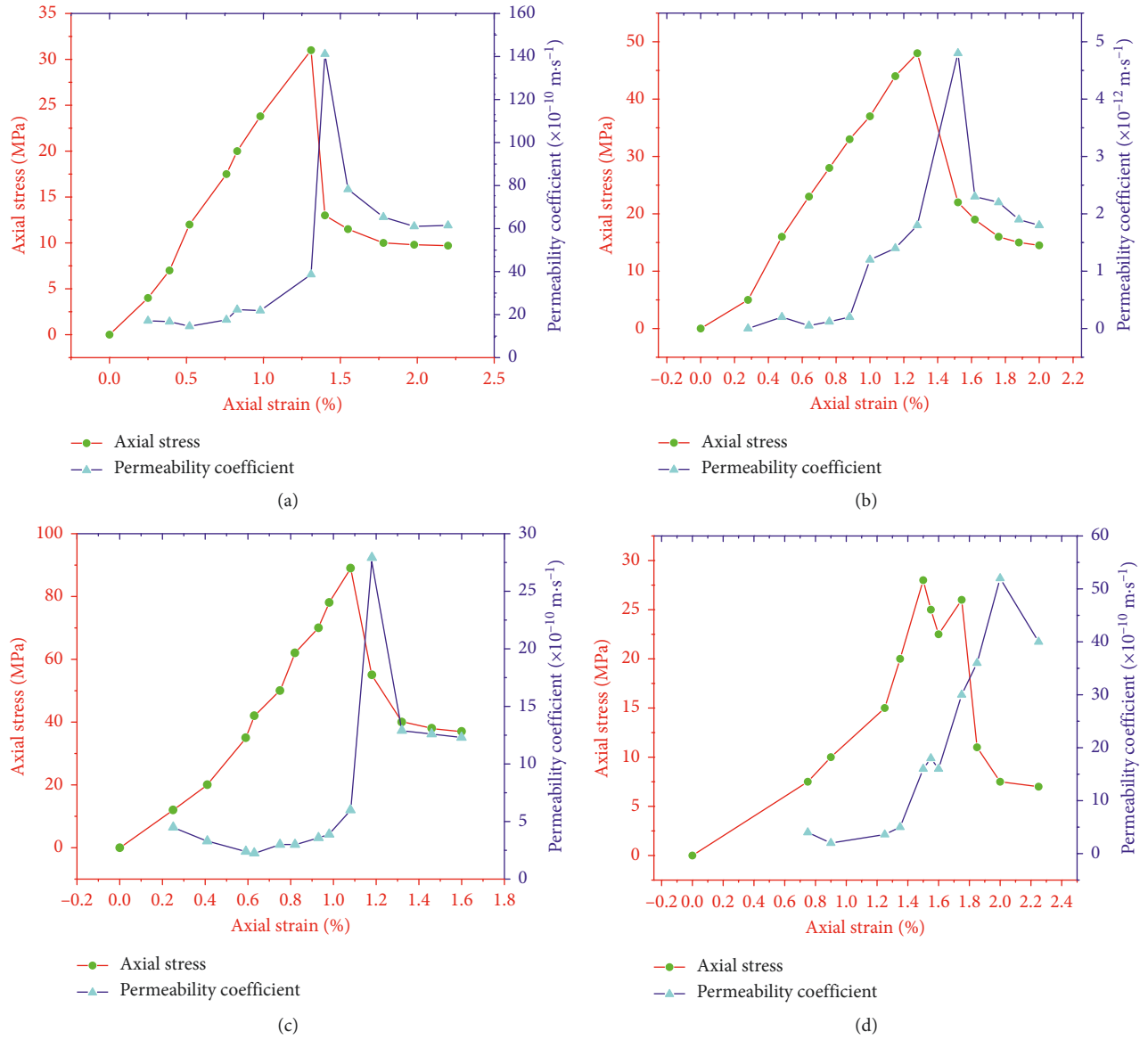

Figure 7: Stress-varying permeability coefficient (K) variation curves for rocks of different lithological properties. (a) Coal. (b) Mudstone. (c) Sandstone. (d) Sandy shale.

effective confining pressure of deep rocks is greater than that of rocks in the upper part. The specific mechanism should be further explored according to concrete rock stresses. For this reason, rock permeability variation rules were explored based on the premises of particular loading paths.

(3) Specific to rock permeability variation rules subjected to particular loading paths, 5 points, below the floor, were selected. For other points of different depths, the relevant research method is the same. During coal mining, the confining pressures in the goaf and the certain space deep in the surrounding floor are different, that is, $\delta 2 \neq \delta 3$. Due to limitations of the experimental instrument, theoretical formula (9) was employed to determine the values of $\delta 1$ and $\delta 2$. Regardless of the squeezing action on the rock from one side, the weak confining pressure should be deemed effective. Such an assumption has no influence on the experimental objectives of the paper. Figure 9 signifies the σ_x, σ_x and τ_{xy} varia0074ions concerned with point M 5 m beneath the floor during working face advance.

The value 120 on the x-axis represents the position of the working face, and point M stands for the position 120 m ahead of the working face and 5 m below the floor. This figure reflects the vertical stress, horizontal stress, and shear stress variation processes of point M when the working face advances from a position 120 m behind M to another position 280 m ahead of it.

One hundred and twenty on the x-axis represents the position of working face and point M stands for a position 120 m ahead the working face and 5 m below the floor. This figure reflects vertical stress, horizontal stress, and shear

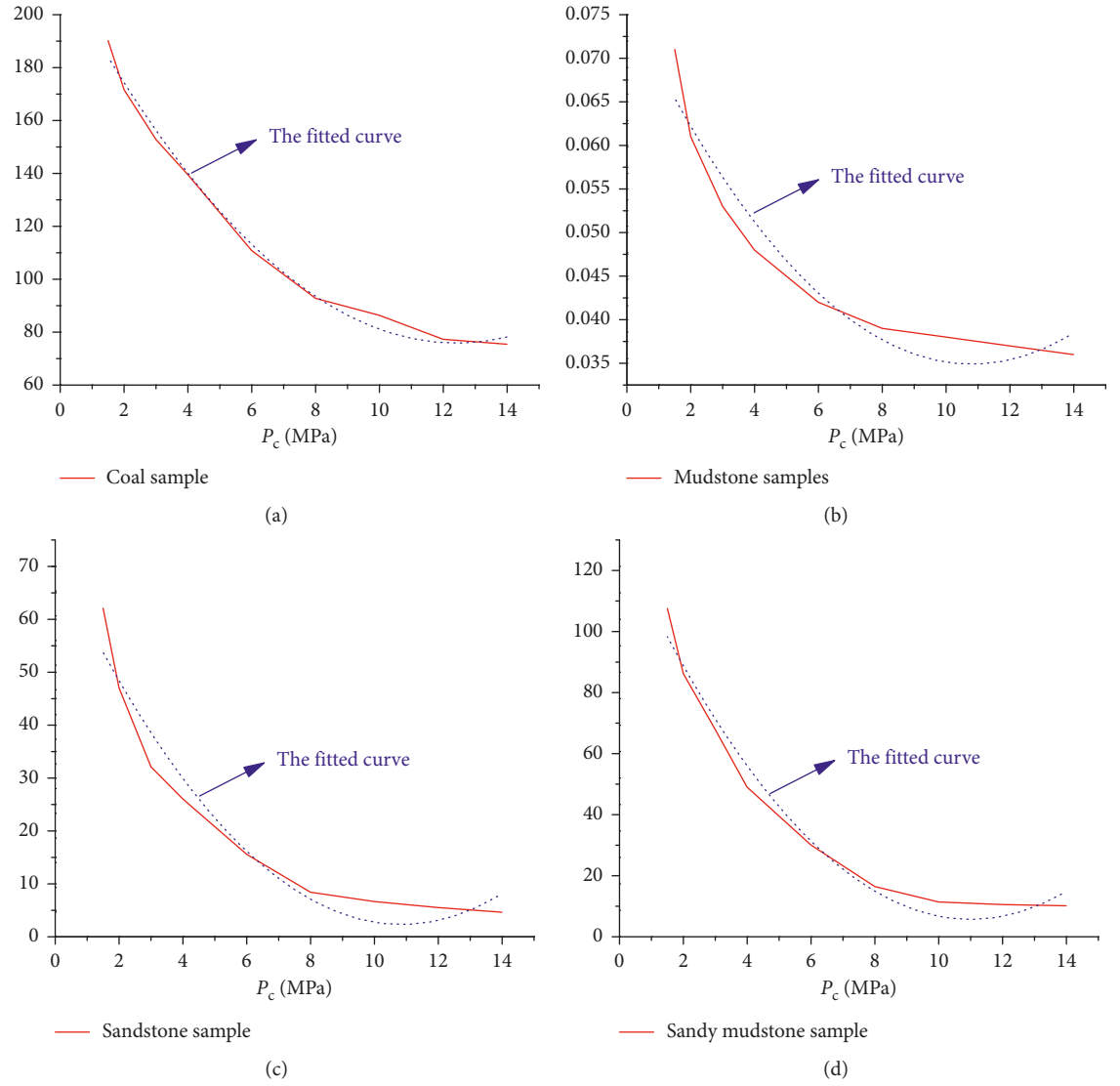

Figure 8: Rock permeability variation rules with different confining pressures.

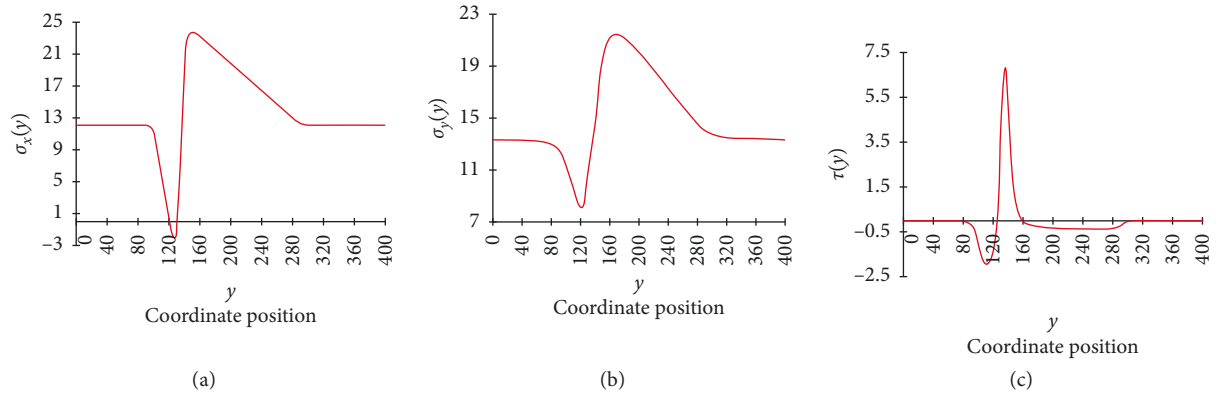

Figure 9: Dynamic stress variation curves of point M. (a) Vertical stress cloud atlas. (b) Horizontal stress cloud atlas. (c) Shear stress cloud atlas.

stress variation processes of point M when the working face advances from a position 120 m behind M to another position 280 ahead it.

Figure 10 signifies maximum principal stress and minimum principal stress variations concerned with point M 5 m beneath the floor during working face advance, that

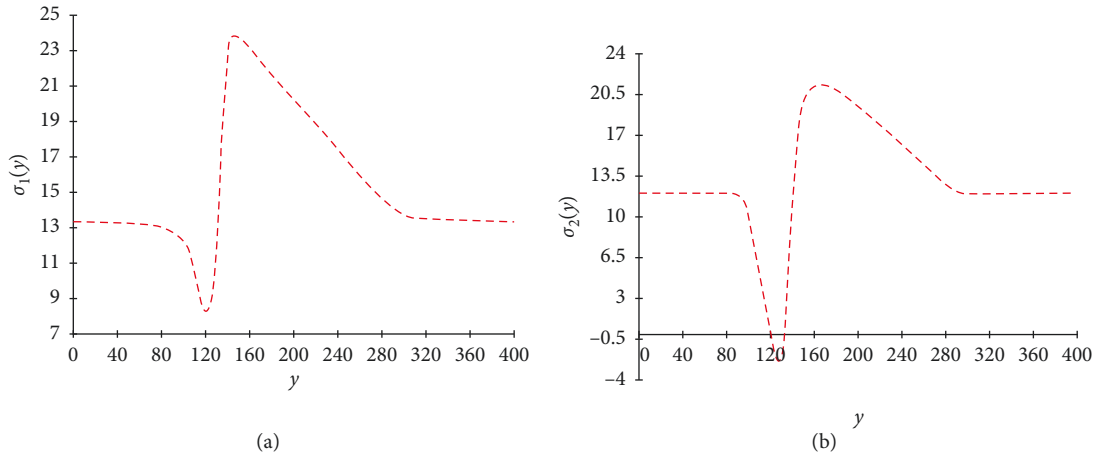

Figure 10: The change of the maximum principal stress and the minimum principal stress along the strike direction at point M. (a) Maximum principal stress. (b) Minimum principal stress.

is, from a point 140 m in front of the working face to another point 260 m behind it. The computational formulae of maximum principal stress σ_1, minimum principal stress σ_2, and $\sigma_x\sigma_x\tau_{xy}$ are given as follows:

$$\sigma_1 = \frac{\sigma_x + \sigma_y}{2} + \sqrt{\left(\frac{\sigma_x - \sigma_y}{2}\right)2 + \tau_{xy}^2},$$
$$\sigma_2 = \frac{\sigma_x + \sigma_y}{2} - \sqrt{\left(\frac{\sigma_x - \sigma_y}{2}\right)2 + \tau_{xy}^2}, \quad (9)$$

where the values of σ_1, σ_2, σ_x, σ_y, and τ_{xy} are obtained by Mathcad, the mining depth is defined to be 500 m, and the specific gravity γ is $2.4{\cdot}10^4$ kN/m^3.

It can be observed from Figure 9(a) that the stress of point M shows a general decreasing tendency followed by an increase before finally recovering to a normal form. When it is approximately 15 m away from the working face, the vertical stress began to decrease sharply and reached zero when the distance was no greater than 15 m. In addition, transient negative pressure would appear below the working face. After the advancement of the working face, the vertical stress would quickly concentrate at 20 m, and the maximum stress increment coefficient would be as high as 2.2. Subsequently, when the advancement of the working face was beyond 160 m, point M would gradually return to the stress of primary rock. The variation laws of the horizontal stress and shear stress are similar to those of the vertical stress, as indicated in Figures 9(b) and 9(c). Due to stress concentration, the rock mass on the seam floor was compressed, while that below the goaf was expanded due to the existence of release space. For this, there is a shear stress increment area between the two zones, which were also the sections with the most substantial rock destruction. The maximum shear stress reached approximately 6.2 MPa, which was 0.47 times the vertical stress of primary rock. It also tilted toward the lower part of goaf, so the stratum thickness would be dramatically reduced by the shear stress, which was one of the most important reasons for water inrush on the floor.

In Figure 10, the position at $y = 120$ of the x-axis stands for the working face. As indicated, the confining pressure within a range of 10 m beneath the working face is negative. The reason is that failure in the rock caving beneath the working face gives rise to a temporary empty-support area in the floor. In addition, the chart of maximum principal stress shows that the maximum principal stress abruptly and continuously climbs to a position 40 m beneath the working face, that is, between 120 and 160 in this chart. Thus, this is an area where the rock compresses under the load, forming the dilation space in it.

Although the maximum principal stress fails to reach the intensity of the rock failure peak, positions 40 m, 20 m, and 5 m in front of the working face and 10 m, 20 m, 40 m, and 100 m behind it were selected as points in the loading path considering that the confining pressure abruptly changes and that the minimum principal stress is negative. The load time for each point was defined to be 1 h. As the confining pressure should be above 1.5 MPa during the laboratory experiment for the purpose of acquiring accurate results, a fitting method was utilized for positions 4 m in front of or 9 m behind the working face. The corresponding outcome is shown in Figure 11.

According to Figure 11, the permeability for areas outside the working face is below 10×10^{-10} m·s^{-1}. Compared with those described in Figure 7, the permeability values in positions within a range of 10 m in front of and 15 m behind the working face exceed 27.9×10^{-10} m·s^{-1}, which is the peak of sandstone in the case of $P_c = 4$ MPa; in addition, the measured maximum value is 92.510×10^{-10} m·s^{-1}. Pursuant to the section of seepage classification for rock-soil bodies specified in the Code for Engineering Geological Investigation of Water Resources and Hydropower of the National Standard of People's Republic of China GB 50487-2008 [32], as shown in Table 1, the lithology of the ground in this area already starts to transform from being impermeable to weakly permeable, which verifies that areas in the range of approximately 5 m in front of and 5 m behind the working face are the most likely to suffer water inrush.

During coal mining, working face advance preferably makes the complete stress-strain process of rocks reappear. The failure zone in the working face gradually changes to

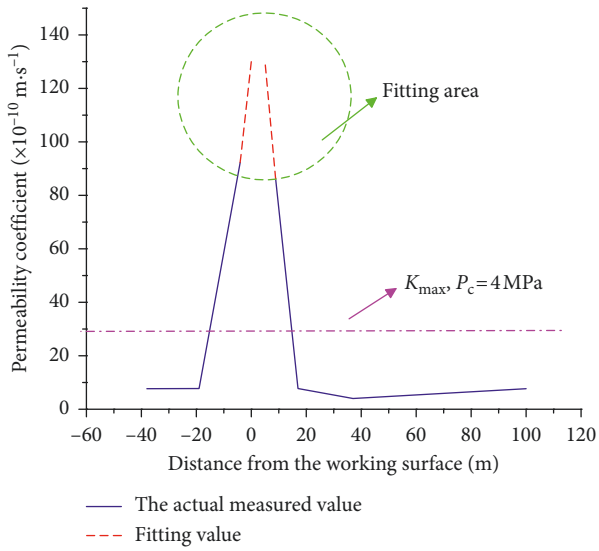

Figure 11: Sandstone permeability variation rules with theoretical computing of confining pressure.

Table 1: Permeability classification of rock-soil bodies.

Grade of permeability	Standard		Soil type
	Permeability coefficient, K (m/s)	Permeability, q (Lu)	
Most impermeable	$K < 10^{-8}$	$q < 0.1$	Clay
Little permeable	$10^{-8} \le K < 10^{-7}$	$0.1 \le q < 1$	Clay-silt
Weakly permeable	$10^{-7} \le K < 10^{-6}$	$1 \le q < 10$	Silt-fine sand
Moderately permeable	$10^{-6} \le K < 10^{-4}$	$10 \le q < 100$	Sand-sand gravel
Strongly permeable	$10^{-4} \le K < 10^{-2}$	$q \ge 100$	Sand gravel-gravel
Very strongly permeable	$K \ge 10^{-2}$		Boulder

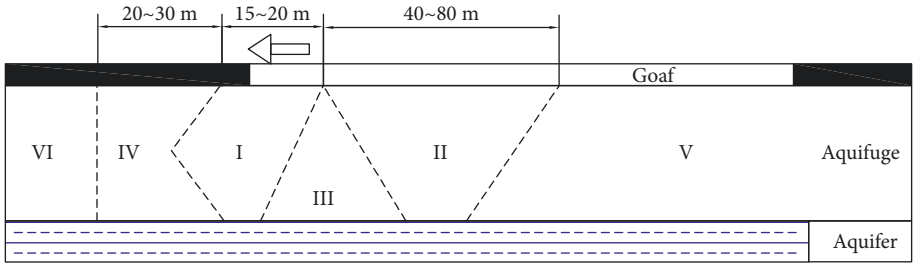

Figure 12: Schematic diagram of floor zonation.

plastic and elastic zones deep in the floor. The strike of the goaf floor also exhibits a tendency toward a compression zone-separation zone and stability restoration zone. According to the opinions of Shi et al. [33–35], floor strata that have been subjected to compression failure in the mine can be divided into four zones from top to bottom. Nevertheless, water inrush only begins first in a certain area during practical production activities. Instead of the entire rock formation, there are usually several water gushing points. Considering this, the goaf floor was classified into 6 zones depending on the likelihood of water inrush occurrence, namely, a compression-expansion zone, a bed separation expansion zone, a pressure relief zone, a compression zone, a stability recovery zone, and a stable zone, as shown in Figure 12.

In ideal conditions, 6 zones of water inrush from seam floor risk were defined in line with rock permeability and rock failure.

Zone I: a compression-expansion zone. Due to the influence of advanced support pressure, rock compression here leads to plastic deformation; meanwhile, mining of the goaf results in stress and volume release space. As the most dangerous area, it is the most likely area for water inrush from the seam floor to occur. The lower parts of positions approximately 5 m in front of and 15 m behind the working face all tilt toward the direction along which the working face advances.

Zone II: a bed separation expansion zone. Under the horizontal squeezing action of advanced support pressure and lateral support pressure, the stress of Zone II is less than that of Zone I. However, an empty-support area is formed temporarily in the roof, or roof falling is extremely insufficient here. As a consequence, rock formation has enough release space so that it is likely that the floor will heave and that separation layers will develop in the formation, which dramatically lowers both the integrity and the water-resisting performance of the rock. Once separation layers and dilation have been formed in the floor, the surrounding rock no longer supports or protects the lower formation, which leads to water inrush risks [36, 37]. In positions with an entire length of approximately 40–80 m at least 15 m beneath the working face in this zone, they exhibit an inverted trapezoidal shape on the whole.

Zone III: a pressure relief zone. Free of highly compressive stress or excessively great tensile stress caused by sideways extrusion, Zone III is under enormous influence from Zones I and II.

Zone IV: a compression zone. Within the range of 25–35 m in front of the working face, the face is influenced by advanced pressure, and the floor is deformed because of compression without dilation. Therefore, the axial pressure and confining pressure here are high. The relevant permeability coefficient is also lower than the normal value of rocks.

Zone V: a stability recovery zone. In the process of gradual compression caused by the goaf collapsing to the rear, floor displacement no longer changes and results in a safe stage at positions approximately 60–100 m beneath the working face.

Zone VI: a stable zone. Independent of any mining-induced influence, it is also an area with the stress of the primary rock.

4. Conclusion

A permeability testing process for rocks subjected to external pressure was presented in this paper together with the application of this process in floor stability estimation. As floor seepage was under the influence of characteristics of the macromechanical environments such as the mine ground pressure, engineering geology, and fluid mechanics, a floor stress model was established to theoretically calculate dynamic variations in the stress during working face advance and to predict the permeability in such stress states. Additionally, rock permeability coefficients in a complete stress-strain process of the rock in the working face floor were sorted in a descending order to categorize the seam floor into 6 zones. In this way, the water-resisting performance of the floor can be represented more objectively.

Data Availability

The data used to support the findings of this study are included within the article. These data were obtained by the authors through experiments.

Conflicts of Interest

The authors declare that there are no conflicts of interest regarding the publication of this paper.

Acknowledgments

The authors gratefully acknowledge the financial support of the National Key Research and Development Program (Grant no. 2016YFC0501102), National Science and Technology Major Project (Grant no. 2016ZX05066-001), and State Key Laboratory of Coal Resources and Safe Mining 2017 Open Fund (Grant nos. SKLCRSM17KFB04 and SKLCRSM17KFA09).

References

[1] Слесарев, *Mine Rock Mechanics and Mine Support*, Fuel Industry Press, Beijing, China, 1954.

[2] C. F. Santos and Z. T. Bieniawski, "Floor design in underground coal mines," *Rock Mechanics and Rock Engineering*, vol. 22, no. 4, pp. 249–271, 1989.

[3] J. Dewu, "Study on Comprehensive Hydrogeological Division of Mazhuang Mine Field in Jiaozuo," *Mining Science and Technology*, vol. 26, no. 2, pp. 1–3, 1998.

[4] W. Xingyi, L. Shifeng, and G. Xu, *Specialized Hydrogeology*, China University of Mining Press, Beijing, China, 2011.

[5] L. Baiying, "Theory and practice to prevent water invasion of coal mine work face," *Mining Geology*, vol. 91, no. 2, pp. 18–38, 1991.

[6] L. Baiying, "Down three zones in the prediction of the water inrush from coilbed floor iquifer theory, development and application," *Shandong Institution.of Mining and Techonology*, vol. 18, no. 4, pp. 11–18, 1999.

[7] L. Baiying, S. Guanghan, and J. Zigang, "Theory and practice of preventing water inrush from mining face," *Safety in Coal Mines*, vol. 5, pp. 47-48, 1988.

[8] W. Hu and L. Yan, "Analysis and consideration on prediction problems of mine water inflow volume," *Coal Science and Technology*, vol. 1, pp. 75–85, 2016.

[9] H. Weiyue and T. Gan, "Mine water disaster type and prevention and control countermeasures in China," *Coal Science and Technology*, vol. 38, no. 1, pp. 92–96, 2010.

[10] H. Weiyue and W. Guangcai, "Development of technique of controlling water hazard on coal mine," *Coal, Geology, and Exploration*, vol. 25, no. S1, pp. 17–23, 1997.

[11] W. Zuoyu, L. Hongquan, W. Pei-Yi, and Y. Shuchun, "Theory and practice of coal mining discipline on confined water," *China Coal Society*, vol. 19, no. 1, pp. 40–48, 1994.

[12] W. Zuoyu and L. Hongquan, *Coal Mining above Confined Aquifer*, China Coal Industry Publishing House, Beijing, China, 1993.

[13] W. Zuoyu and L. Hongquan, "Analysis on critical anti-hydropressure ability for the remaining intact rock of floor," *Chinese Journal of Rock Mechanics and Engineering*, vol. 13, no. 4, pp. 319–326, 1994.

[14] Q. Minggao, M. Xiexing, and X. Jianlin, "Theoretical study of key stratum in ground control," *Journal of China Coal Society*, vol. 21, p. 225, 1996.

[15] L. Liangjie, Q. Minggao, and L. Shugang, "Mechanism of water-inrush through fault," *Journal of China Coal Society*, vol. 21, no. 2, pp. 119–123, 1996.

[16] Q. Wu, Y. Liu, D. Liu, and W. Zhou, "Prediction of floor water inrush: the application of GIS-based AHP vulnerable index method to Donghuantuo Coal Mine, China," *Rock Mechanics and Rock Engineering*, vol. 44, no. 5, pp. 591–600, 2011.

[17] Q. Wu, D. Zhao, Y. Wang, J. Shen, W. Mu, and H. Liu, "Method for assessing coal-floor water-inrush risk based on the variable-weight model and unascertained measure theory," *Hydrogeology Journal*, vol. 25, no. 7, pp. 2089–2103, 2017.

[18] S. Peng, L. Luo, and J. Wang, "Determination of rational staggered distance in double-longwall faces in mining on confined aquifer," *Journal of Rock Mechanics and Engineering*, vol. 22, no. 1, pp. 48–52, 2003.

[19] Z. Huang, Z. Jiang, X. Tang, X. Wu, D. Guo, and Z. Yue, "In situ measurement of hydraulic properties of the fractured zone of coal mines," *Rock Mechanics and Rock Engineering*, vol. 49, no. 2, pp. 603–609, 2015.

[20] Z. Meng, G. Li, and X. Xie, "A geological assessment method of floor water inrush risk and its application," *Engineering Geology*, vol. 143-144, no. 4, pp. 51–60, 2012.

[21] Y. Wang, X. Yin, H. Jing, R. Liu, and H. Su, "A novel cloud model for risk analysis of water inrush in karst tunnels," *Environmental Earth Sciences*, vol. 75, no. 22, p. 1450, 2016.

[22] D. Ma, M. Rezania, H. S. Yu, and H. B. Bai, "Variations of hydraulic properties of granular sandstones during water inrush: effect of small particle migration," *Engineering Geology*, vol. 217, pp. 61–70, 2016.

[23] N. Kang, Q. B. Luo, S. Chen, L. I. Gui-Juan, and L. V. Guang-Luo, "Analysis of mine inflow drainage and its impact on the groundwater flow field in the water-inrush-dangerous areas in coal mine," *Ground Water*, vol. 38, pp. 26–29, 2016.

[24] W. X. Wang, W. H. Sui, B. Faybishenko, and W. T. Stringfellow, "Permeability variations within mining-induced fractured rock mass and its influence on groundwater inrush," *Environmental Earth Sciences*, vol. 75, no. 4, p. 326, 2016.

[25] X. L. Liu, G. Han, E. Wang, S. Wang, and K. Nawnit, "Multiscale hierarchical analysis of rock mass and its mechanical and hydraulic properties prediction," *Journal of Rock Mechanics and Geotechnical Engineering*, vol. 10, no. 4, pp. 694–702, 2018.

[26] Y. P. Guan, X. L. Liu, E. Wang, S. Wang, S. Wang, and J. Zhong, "Quantitative characterization method for the microcontacts and macrocontacts of two-dimensional granular materials," *International Journal of Geomechanics-ASCE*, vol. 18, no. 4, article 04018016, 2018.

[27] M. Li, J. X. Zhang, Y. L. Huang, and R. Gao, "Measurement and numerical analysis of influence of key stratum breakage on mine pressure in top-coal caving face with super great mining height," *Journal of Central South University*, vol. 24, no. 8, pp. 1881–1888, 2017.

[28] D. F. Malan, "Time-dependent behaviour of deep level tabular excavations in hard rock," *Rock Mechanics and Rock Engineering*, vol. 32, no. 2, pp. 123–155, 1999.

[29] S. H. Oh, K. S. Lee, W. M. Jeong, S. A. Kalogirou, and P. Christodoulides, "Three-dimensional experiment and numerical simulation of the discharge performance of sluice passageway for tidal power plant," *Renewable Energy*, vol. 92, pp. 462–473, 2016.

[30] K. Bisdom, G. Bertotti, and F. H. Bezerra, "Inter-well scale natural fracture geometry and permeability variations in low-deformation carbonate rocks," *Journal of Structural Geology*, vol. 97, pp. 23–36, 2017.

[31] S. Peng, Z. Meng, H. Wang, C. Ma, and J. Pan, "Testing study on pore ratio and permeability of sandstone under different confining pressures," *Chinese Journal of Rock Mechanics and Engineering*, vol. 22, no. 5, pp. 742–746, 2003.

[32] Ministry of Water Resources People's Republic of China, *Water Conservancy and Hydropower Engineering Geological Survey Specification*, Water Conservancy and Electric Power Press, Beijing, China, 2009.

[33] C. Jiulong, L. Li, S. Longqing et al., *Application of New Geophysical Technology in Coalmine Safety Monitoring*, in *Proceedings of International Symposium on Safety Science and Technology*, Shangdong, China, 2002.

[34] L. Shi, *Summary of Research on Mechanism of Water-Inrush from Seam Floor*, Shandong University of Science and Technology, Qingdao, China, 2009.

[35] L. Shi, M. Qiu, W. Wei, D. Xu, and J. Han, "Water inrush evaluation of coal seam floor by integrating the water inrush coefficient and the information of water abundance," *International Journal of Mining Science and Technology*, vol. 24, no. 5, pp. 677–681, 2014.

[36] H. Wagner, *The New Austrian Tunneling Method*, Technology and Potential of Tunnelling, South African Tunnelling Conference, South Africa, 1970.

[37] K. P. Lorna, "Tunnelling method and apparatus," US3407609, 1968.

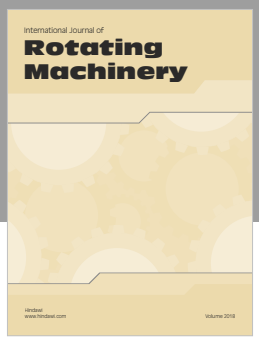

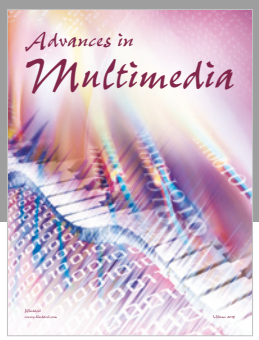

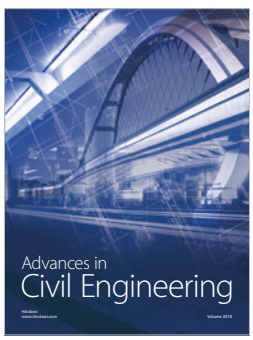

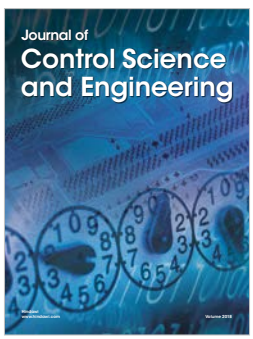

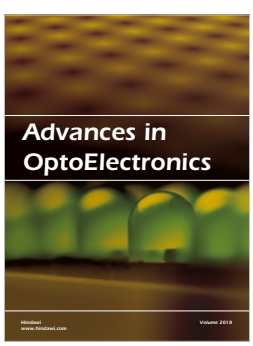

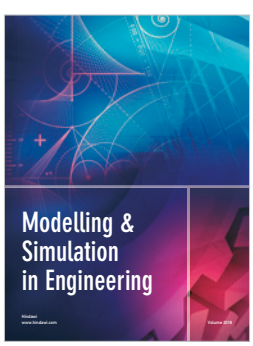

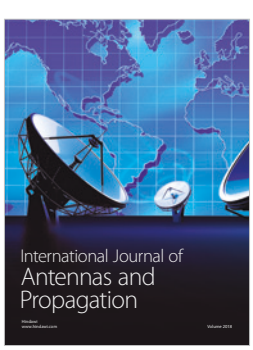

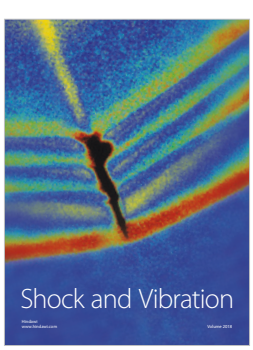

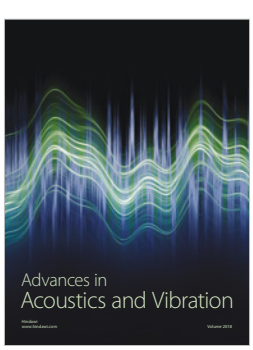

Hindawi

Submit your manuscripts at
www.hindawi.com